Modelling and simulation of vibrationnal properties of carbon nanotubes and derivatives

A. Rahmani, K. Sbai, H. Chadli and J.-L. Sauvajol*

Equipe de Physique Informatique et Modélisation des Systèmes, Université MY Ismail, Faculté des Sciences, BP 11201, Zitoune, 50000 Meknès, Morocco
** Laboratoire des Colloïdes, Verres et Nanomatériaux (UMR CNRS 5587),CP026, Université Montpellier II, 34095 Montpellier Cedex 5, France*

Corresponding author: abd.rahmani@menara.ma

The aim of the present paper is to identify the main Raman vibrational features of carbon nanotubes and derivatives. In this goal, Raman active mode calculations have been performed on different single-walled carbon nanotubes (SWCNTs) and double-walled carbon nanotubes (DWCNTs) as well as peapods. The comparison between the calculations performed on these different systems allows us to identify the Raman-active modes of each carbon nanomaterials. In SWCNTs, the tangential modes are located around 1590 cm^{-1} and the radial breathing mode follows A/D law. This latter law is modified in bundle of SWCNTs, DWCNTs or peapods.

Keywords: Nanotube, Nanopeapod, Fullerene, Raman spectroscopy, spectral moment method.

I. INTRODUCTION

Since the discovery of carbon nanotubes [1], much attention has been devoted to the investigation of their vibrational properties, experimentally as well as theoretically. Resonant Raman scattering technique has been shown to provide a powerful tool for studying the phonon dynamic of single-walled carbon nanotubes (SWCNTs) [2, 3].

Obviously, the use of Raman spectroscopy to study the SWCNT chemistry implies the knowledge of the Raman intrinsic vibrational modes of SWCNTs. The aim of the present investigation is to identify the intrinsic Raman features of carbon materials.

For instance, three modes located around radial, default and tangential modes have been reported. Very recently, a Raman investigation was performed on thin films of SWCNT bundles. By contrast with all the previous studies, a larger number of lines were observed in this latter investigation. The sharp lines in the Raman spectra of these purified and annealed SWCNTs were assigned to one- and two-phonons modes [4]. In summary, a large disagreement is found in the literature concerning the assignment of the Raman-active modes of SWCNTs. On the other hand, the Raman-active phonon modes of SWCNTs have been calculated from different methods: zone folding model [5, 6, 7], tight binding approach [8], force constant model [9, 10, 11] and *ab-initio* calculations [12]. Concerning the diameter dependence of the Raman active modes these predictions are sometimes opposite.

In previous paper [13], using the spectral moment's method [14, 15], in the framework of the bond-polarization theory we have calculated the polarized Raman spectra of chiral and achiral SWCNTs as function of their diameter and length. An investigation of finite-size effects was extended to a large of finite lengths up to 85 nm as well as to achiral and chiral tubes of several diameters. The dependence of tangential modes on chirality and the dependence of the Raman spectrum on the tube length were clearly observed.

The main aim of the present paper is to identify unambiguously the Raman features of carbon nanomaterials. In this goal, Raman calculations have been performed on different well-defined SWCNTs and DWCNTs as well as peapods and bundling effects. The non-resonant Raman active modes were calculated for several diameters, chiralities and lengths for these carbon nanomaterials, using the spectral moment's method (SMM).

II. MODELS AND METHOD

1. Structure

Let us recall that the ideal nanotube structure can be obtained from graphene sheet by rolling it up along the straight line connecting two lattice points into a seamless cylinder in such a way that the two points coincide [16]. The tube can be specified by integers (n,m) that define the translation vector between the two points. Alternatively, the tube can be described by its diameter D and the chiral angle θ which is the angle between the tube circumference and the nearest zigzag of carbon-carbon bonds. The tube is called

achiral for θ = 0° (zigzag type) and θ =30° (armchair type), and chiral for 0°< θ < 30°.

A double-wall carbon nanotube is a special case of multiwall tubes consisting of only two concentrics SWCNTs. The DWCNT walls are assumed to be at a distance d close to 0.34 nm and whose diameters are D_i=D and D_{out}=D+d. Let us note that DWCNT is made up of an internal tube (n, m) and an external tube (k,l) as (n,m)≅(k,l).

A carbon peapod consists of C_{60} molecules trapped inside a SWCNT host. The configuration of the guest molecules within the nanotube has already been found to be diameter dependent [17,18]. In this study, we consider SWCNTs with diameters ranging from 1.25 nm to 2.20 nm in which the C_{60} molecules phase can take a linear or a zigzag configuration depending on the diameter. The energy calculations were performed using a Lennard-Jones potential to describe the van der Waals interactions between both adjacent fullerene molecules and, on the other hand, between fullerenes and the nanotube.

When nanotubes (SWCNTs, DWCNTs or peapods) are closely packed together, a three dimensional bundle is formed. From the diffraction profile of the crystalline ropes of CNT, it has been previously reported that these systems can be represented by two dimensional infinite hexagonal lattices of uniform cylinders [19]. For finite-size bundle, the nanotubes were placed parallel one to each others on a finite-size hexagonal array of cell parameter, $a_0=D_t+d_{t-t}$, where d_{t-t} represents the intertube spacing. The intertube interaction energy is minimised with respect to the intertube separation and the angle of simultaneous rotation of all tubes about their axes. The optimized intertube separations are roughly equal to 0.32 nm. This value, slightly smaller than the inter-graphene sheets distance in graphite, is in agreement with calculations [20,21] and experiments [22]. The number of tubes per bundle is called N_t

2. Dynamics

It is well known that in the elements of the dynamical matrix, $\widetilde{D}$, are given by:

$$D_{\alpha\beta}(n,m) = \frac{1}{\sqrt{M_n M_m}}\phi_{\alpha\beta}(n,m) \quad \text{with}$$

$$\phi_{\alpha\beta}(n,n) = -\sum_m \phi_{\alpha\beta}(n,m)$$

where $\phi_{\alpha\beta}(n,m)$ are the force constants between the n and m atoms. The interactions are restricted only to the first, second, third and fourth nearest neighbours. So, only four 3x3 force-constant matrices are required to generate the dynamical matrix of the SWCNT [7].

In this work, to describe the coupling between vibrational modes and photons, we use the non-resonant bond-polarisation theory [23,24]. In this approach, the polarizability is modelled in terms of bond contributions as:

$$\pi_{\alpha\beta} = \frac{1}{3}(2\alpha_p + \alpha_l)\delta_{\alpha\beta} + (\alpha_l - \alpha_p)\left(\hat{r}_\alpha \hat{r}_\beta - \frac{1}{3}\delta_{\alpha\beta}\right)$$

where $\hat{r} = \hat{r}_j - \hat{r}_i$ is a vector which defines the direction and the distance of a pair of nearest neighbour atoms at sites $\hat{r}_i$ and $\hat{r}_j$. The parameters α_l and α_p correspond to the longitudinal and perpendicular bond polarizability, respectively. The derivatives $\pi^n_{\alpha\beta,\gamma}$ are given by:

$$\pi_{\alpha\beta,\gamma} = \frac{1}{3}(2\alpha'_p + \alpha'_l)\delta_{\alpha\beta}\hat{r}_\gamma + (\alpha'_l - \alpha'_p)\left(\hat{r}_\alpha \hat{r}_\beta - \frac{1}{3}\delta_{\alpha\beta}\right)\hat{r}_\gamma + \frac{\alpha_l - \alpha_p}{r} \times \left(\delta_{\alpha\gamma}\hat{r}_\beta + \delta_{\beta\gamma}\hat{r}_\alpha - 2\hat{r}_\alpha \hat{r}_\beta \hat{r}_\gamma\right)$$

where $\hat{r}$ is a unit vector along r and $\alpha'_l = (\partial\alpha_l/\partial r)_0$ and $\alpha'_p = (\partial\alpha_p/\partial r)_0$.

In SWCNT one bond type occurs and the bond polarizability model is completely defined by three parameters: $\alpha = 2\alpha'_p + \alpha'_l$, $\beta = \alpha'_l - \alpha'_p$ and $\gamma = \alpha_l - \alpha_p$. These parameters are usually obtained by fitting the experimental intensities. The empirical parameters used in this study are $\alpha = 4.7\,\text{Å}^2$, $\beta = 4.0\,\text{Å}^2$ and $\gamma = 0.04\text{Å}^3$.

We consider that intertube interaction is represented by the force constants set used in our previous paper concerning the Raman spectra in SWCNTs [13]. A Lennard-Jones potential, $U_{LJ} = 4\varepsilon\left(\frac{\sigma}{R^{12}} - \frac{\sigma}{R^6}\right)$, is used to describe the carbon-carbon long range interaction in order to take into account the intertube interactions. The Van Der Waals parameters are ε = 2.964 mev and σ = 0.3407 nm. To describe the coupling between vibrational modes and photons, we use the non-resonant bond-polarizability model. For CNT bundles, we neglect the lattice effect on the bond-polarizability model parameters.

A usual method to calculate the Raman spectrum requires, besides the polarization parameters, the eigenvalues and the eigenvectors which can be obtained by direct diagonalization of the dynamical matrix of the system. However when the system contains a large number of atoms, as for long finite CNT systems, the dynamical matrix is very large and its diagonalization fails or requires long computing time. The spectral moment's method allows us to compute directly the Raman

spectrum of very large harmonic systems without any diagonalization of the dynamical matrix [13,14,15].

III. RESULTS AND DISCUSSION

Using the spectral moment's method, the Raman active-mode frequencies are directly obtained from the position of the peaks in the calculated Raman spectra (the line width of each peak was fixed at 1.7 cm^{-1}). The intensity of the Raman spectrum is normalized with respect to the number of carbon in the sample under consideration. In our calculations, the axes of the tubes are along the Z axis, and a carbon atom of each tube is along the X axis of the CNT reference frame. The laser beam is kept along the y axis of the reference frame. We consider that both incident and scattered polarizations are along the z axis to calculate the polarized ZZ spectra. More than 25000 atoms in carbon nanotubes were treated.

1. SWCNTs

Firstly, the calculations are performed on infinitely isolated and bundles (crystals) of SWCNTs of several diameters. Shifts for A_{1g} modes are observed when the tube diameter increases. In the BLM region, the ZZ spectra exhibit two peaks denoted here as RBLM (for radial breathing-like mode) and BBLM (for bundle breathing-like mode). The comparison between the Raman spectra of the SWCNTs and BWCNTs shows the appearance of a second mode (BBLM) at a frequency higher than that of RBLM one. For all modes, we observe a downshift with increasing tube diameter. One can see that for small nanotube diameter, only the RBLM has an important intensity and this mode is associated with a nearly pure breathing like eigenvector. This RBLM mode is the mode that has been reported in different studies [25, 26, 27]. To illustrate the BLM frequencies dependence with nanotube diameter, we have reported in figure 1, the frequency of A_{1g}^{S}, E_{1g}^{S}, E_{2g}^{S} for SWCNTs (open symbols), RBLM and BBLM for BWCNT's (solid symbols) in terms of nanotube diameter D. For SWCNTs, we show that the frequency modes obey to the A/R$^{\alpha}$ law, with α close to 1 and A=157, 481 and 225 $cm^{-1}nm^{-1}$ for E_{1g}^{S}, E_{2g}^{S} and A_{1g}^{S} modes, respectively. The latter value is close to the values obtained by other works. One can observe that this linear relationship between inverse tube diameter and the RBM mode frequencies stated for SWCNT's was affected by the presence of neighbouring tubes. The evolution of the BWCNT frequency modes E_{1g}^{b} and E_{2g}^{b} is characterized by coefficients A and α different from those found in the case of SWCNT's: A= 134 and 475 $cm^{-1}nm^{-1}$ with α=0.86 and 0.97 for E_{1g}^{b} and E_{2g}^{b}, respectively. The variation of the frequency of RBLM and BBLM according to the diameter of the tube seems characterized by two sets of parameters: when $D < D_c$, we obtain values of A= 212 and 622 $cm^{-1}nm^{-1}$ with α= 0.92 and 1.31, whereas, when $D > D_c$, these values are close to A= 512 and 187 $cm^{-1}nm^{-1}$ with α= 1.35 and 0.75 for RBLM and BBLM modes, respectively. The calculated D_c value is close to 2.75 ± 0.25 nm. Concerning the Raman intensity, we observe a decrease of the intensity with the increase in the diameter, except for the BBLM mode. If we consider the variation of the Raman intensity ratio I_{BBLM}/I_{RBLM}, we observe a growth of this ratio, if when the diameter of tube increases to reaches value 1 for diameter close to D_c.

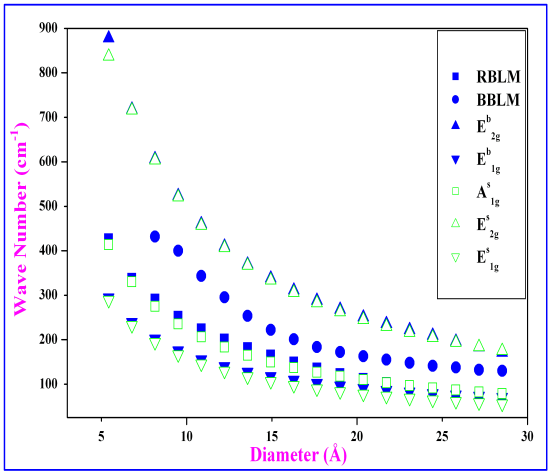

Fig. 1: Diameter dependence of the Raman-active modes frequencies for SWCNT crystals.

2. DWCNTs

The calculations are performed on infinite DWCNTs of different diameters and chiralities. To obtain infinite DWCNTs we applied periodic boundary conditions on unit cells of the considered nanotubes forming the system. The results for a typical armchair DWCNTs showed that, in TM region, spectra present six peaks corresponding to two A_{1g}, E_{1g}, E_{2g} triplet modes for (n,m) and (k,l) tubes, respectively. In addition, when the tube diameter increases, we observe an upshift for A_{1g} and E_{1g} modes and a downshift for E_{2g} mode to form, for larger tubes, a single larger band around 1582 cm^{-1}. As for TM region, the RBM one present two triplet modes associated to A_{1g}, E_{1g} and E_{2g} for each internal and external tubes of the system. As it can be seen in figure 2, where we have represented the outer tube diameter versus frequency, we observe a downshift for RBM modes and a globally upshift of TM modes with increasing diameter. In comparison with SWCNT Raman spectra, we note

that the RBM region of DWCNTs is characterized by an upshift of the frequency modes. The TM region of SWCNTs is slightly affected by the DWCNT packing.

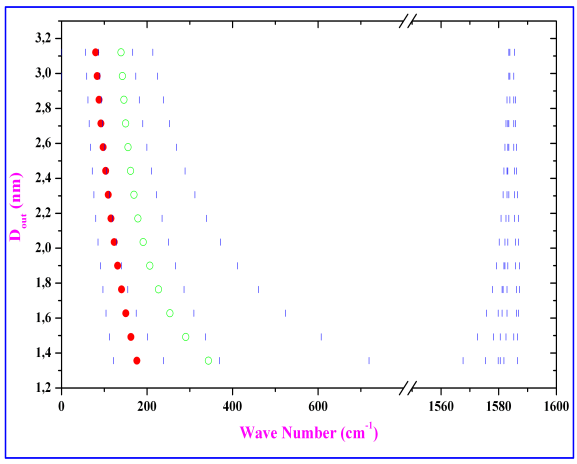

Fig. 2: Diameter dependence of the Raman-active mode frequencies for $(n,n)\cong(n+5,n+5)$ DWCNT's. Low-frequency RBLM's (solid circle) and high-frequency RBLM's (open circle). Ref. [29].

The position of the high-frequency RBLM, ω_{HF}, is well fitted by the analytical expression: ω_{HF} (cm^{-1})= $A_i/D_{inner}+ B_iD_{inner} + C_i$, with parameters close to A_i=225 cm^{-1} nm, B_i=20.6 cm^{-1} nm^{-1} and C_i=−2.4 cm^{-1}. On the other hand, the dependence of the position of the RBLM's of lowest frequency, ω_{LF}, is well fitted by the relation: ω_{LF} (cm^{-1}) = $A_o/D_{outer}^2 + B_o/D_{outer}+ C_o$, with parameters close to A_o=−88.8 cm^{-1} nm^2, B_o=324.1 cm^{-1} nm and C_o=−14.7 cm^{-1}.

It must be emphasized that these previous expressions only have a useful interest to relate the diameter of tubes and the experimental RBLM frequencies [28]. No physical meaning is attached to the values of the different parameters of the fit.

In comparison with the diameter dependence of the RBM frequency in isolated SWCNTs, different behaviour is found for both the RBLM's in DWCNT's. In the diameter range of inner tubes, 0.6–2.4 nm, the frequency shift of the highest frequency RBLM's with respect to the position of the RBM's of the isolated inner tube is found to depend linearly on the inner tube diameter (Fig. 3). In contrast, in the related diameter range of the outer tubes: 1.2–3 nm, we found that the shift of the low-frequency RBLM's with respect to the RBM frequency of the isolated outer tube is no longer linear (Fig. 3). For very small diameters, the shift is linear. The change in the shift behaviour occurs around 1.7 nm. For the small diameters, each of the two RBLM's has the characteristic features of the RBM of one of the tube. In contrast, for large diameter (above 1.7 nm in our work), the low- and high-frequency RBLM's are in-phase and counterphase collective motions of both tubes, respectively. The dependencies of the RBLM frequencies as a function of the diameter (Figs. 2 and 3) are close to those found in recent and different approaches.

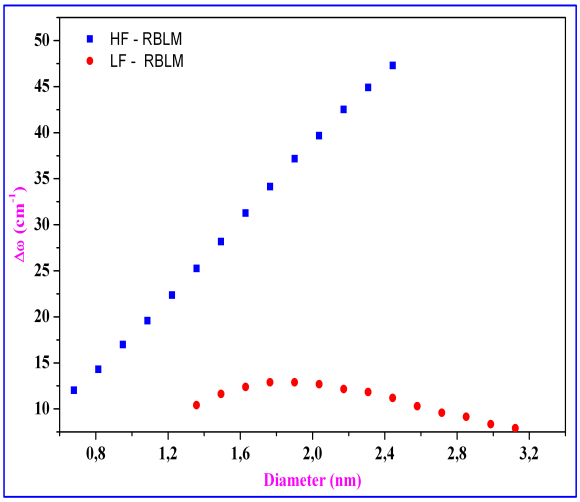

Fig. 3: Dependence of the gap between RBLM and RBM as a function of the tube diameter for $(n,n)\cong(n+5,n+5)$ DWCNT's. High-frequency RBLM's (solid square) and low-frequency RBLM's (solid circle). See Ref. [29].

3. Peapods

In the following, Raman spectra have been calculated on individual oriented peapods. We focus on the BLM region of the *ZZ* polarized Raman spectrum. We have investigated the dependence of some specific Raman active modes of infinite peapods as a function of the diameter of the nanotube. Figure 4 shows the evolution of the RBM and RBLM frequencies as a function of the tube diameter. The RBLM of linear (diameter below 1.45 nm) and zigzag (diameter between 1.45 and 2.17 nm) peapods show distinct behaviors. The behavior of the RBLM in linear peapods is qualitatively the same as those of the RBM. However, it deviates from the scaling law stated for the RBM frequency. For zigzag peapods, we already reported the splitting of the RBM into two components. For tubes having a diameter smaller than D_c=1.78 nm, associated to angles θ greater than θ_c=120°, the high- and low-frequency component of RBLM doublet, called RBLM1 and RBLM2 in the following, downshift when the tube diameter increases. Note that the slopes of the variations are different. By contrast, for tubes having a diameter greater than D_c=1.78 nm, associated to angles θ lower than θ_c, the low (high)-frequency component of RBLM doublet downshifts (upshifts) when the diameter increases. In the inset of Fig. 4, we have reported the variation of the Raman intensities of the two components of the RBLM as a function of the nanotube diameter. The

ratio $r=I_{RBLM1}/I_{RBLM2}$ is equal to 1 for $D=D_c$ ($\theta=\theta_c$), $r>1$ for $D<D_c$ ($\theta>\theta_c$) and $r<1$ for $D>D_c$ ($\theta<\theta_c$). When θ reaches 180° (60°), the ratio $r>>1$ ($r<<1$) and the low frequency region is dominated by the component of the RBLM doublet located at the frequency the closest of the frequency of the RBM. The frequency and intensity behaviours of the RBLM1 and RBLM2 suggest an exchange from one mode to the other associated to an anticrossing effect of the dispersion curves of the RBLM1 and RBLM2 with the diameter in zigzag peapods.

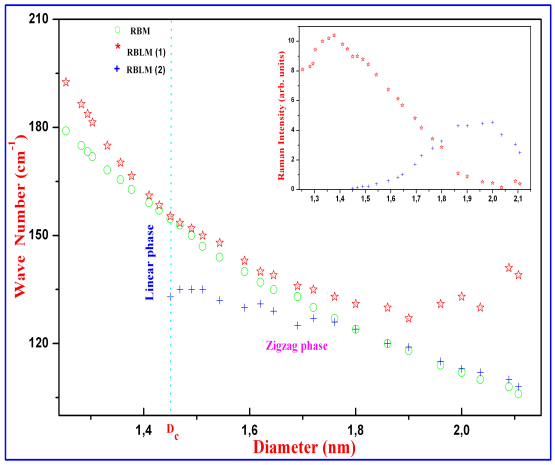

Fig. 4: The diameter dependence of the RBLM frequency in *linear* and *zigzag peapods*: RBLM1 (star) and RBLM2 (cross). The diameter dependence of the RBM for the related empty tubes is also displayed (open circles). The limit (D_c, see text) between *linear* and *zigzag peapods* is identified by the vertical dashed line. Inset: the corresponding intensities of the RBLM1 and RBLM2 versus the diameter of the nanotubes. See Ref. [30].

IV. Conclusion

The spectral moment's method was used to calculate the polarized nonresonant Raman spectra for achiral and chiral single-wall carbon nanotubes in a large diameter and length range. The analysis of results in the light of diameter and chirality dependence performed on SWCNT's samples shows the good agreement with our model. Thanks to the spectral moment's method, we have investigated bundles consisting of more than 100 SWCNT's of several sizes.

We have calculated the nonresonant Raman spectrum of isolated DWCNT's. The dependence of the spectrum with the diameter of the inner and outer tubes of isolated DWCNT has been analyzed. Expressions are derived to describe the dependence with the diameter of the RBLM's in isolated infinite DWCNT's. These expressions can be used to experimentally derive the inner and outer tube diameters from the measurement of the RBLM frequencies. These expressions are valid for tubes longer than 40 nm, and they can be used to interpret the majority of the experiments on DWCNT's. General good agreement is found between predictions and experimental values [30].

We have calculated the nonresonant Raman spectrum of isolated peapods. For the tube diameter investigated range, the C_{60} molecules adopt a linear arrangement for SWCNTs diameter lower than 1.45 nm, and a zigzag configuration for diameters between 1.45 nm and 2.20 nm. Both for the obtained *linear* and *zigzag peapods*, the dependence of the Raman spectrum with the diameter have been analyzed. We found that the behavior of the RBLM mode with the SWCNT diameter was clearly modified in peapods. Therefore, the linear relation between the RBLM wave number and the inverse of diameter found in SWCNT will be modified in the peapod.

Acknowledgements

The work was supported by a CNRS-France/CNRST-Morocco agreement.

BIBLIOGRAPHY

[1] S. Iijima, Nature (London), **354**, 56 (1991)
[2] M. S. Dresselhaus and P. C. Eklund, Advances in Physics **49**, 705 (2000)
[3] S. Reich, C. Thomsen, and J. Maultzsch: Carbon nanotubes. Basic Concepts and Physical Properties (Wiley-VCH, Weinheim, Germany 2004)
[4] U. J. Kim, X. M. Liu, C. A. Furtado, G. Chen, R. Saito, J. Jiang, M. S. Dresselhaus , and P. C. Eklund, Phys. Rev. Lett. **95**, 157402 (2005)
[5] R. A. Jishi, L. ven Kataraman, M. S. Dresselhaus, and G. Dresselhaus, Chem. Phys. Lett. **209**, 77 (1993).
[6] P. C. Eklund, J. M. Holden, and R. A. Jishi, Carbon **33**, 959 (1995)
[7] R. Saito, T. Takeya, T. Kimura, G. Dresselhaus, and M.S. Dresselhaus , Phys. Rev. B **57**, 4145 (1998)
[8] D. Kahn and Jian Ping Lu , Phys. Rev. B **60**, 6535 (1999)
[9] V. N. Popov, V. E. van Doren, and M. Balkanski, Phys. Rev. B **59**, 8355, 1999; Phys. Rev. B **61**, 3078, (2000)
[10] M. Damnjanovic, I. Milosevic, T. Vukovic, and R. Sredenovic, Phys. Rev. B **60**, 2728 (1999)
[11] E. Dobardzic, I. Milosevic, B. Nikolic, T. Vukovic, and M. Damnjanovic, Phys. Rev. B **68**, 045408 (2003)
[12] O. Dubay and G. Kresse, Phys. Rev. B **67**, 035401 (2003)
[13] A. Rahmani, J.L. Sauvajol, S. Rols and C. Benoit, Phys. Rev. B **66**, 125404 (2002).
[14] C. Benoit, E. Royer and G. Poussigue, J. Phys.: Condens. Matter 4, 3125 (1992).

[15] A. Rahmani , P. Jund, C. Benoit and R. jullien, J. Phys. Condens. Matter 13, 5413, (2001).
[16] R. Saito, M. Fujita, G. Dresselhaus, and M.S. Dresselhaus Phys. Rev. B **47**, 16 671 (1992).
[17] Miroslave Hodak and L. A. Girifalco, Phys. Rev. B **68**, 085405 (2003).
[18] Miroslave Hodak and L.A. Girifalco, Phys. Rev. B **67**, 75419 (2003).
[19] S. Rols, R. Almairac, L. Henrard, E. Anglaret, J.L. Sauvajol, Eur. Phys. J. B 10, 263 (1999).
[20] J. C. Charlier, X Goze, JP Michenaud, Europhys. Lett. **29**, 43 (1995).
[21] L. Henrard, V.N. Popov and A. Rubio, Phys. Rev. B. **64**, 205403 (2001).
[22] A Thess, R. Jee, P. Nikolaev, H. Dai, P. Petit, J. Robert, C. Xu, Y. Hee Lee, S. Gon Kim, AG Rinzler, DT Colbert, GE Scuseria, D. Tomanek, JE Fisher, R.E Smalley, Sience 273, 483 (1996).
[23] R. J. Bell, Methods in Computational Physics, Vol. 15, Academic,New York, (1976).
[24] S. Guha, J. Menendez, J. B. Page, and G. B. Adams, Phys. Rev. B **53**, 13106 (1996).
[25] L. Henrard, E. Hernandez, P. Bernier, and A. Rubio, Phys. Rev. B. **60**, R8521 (1999).
[26] D. Kahn and J.P. Lu, Phys. Rev. B. **60**, 6535 (1999).
[27] U. D. Venkateswaran, A.M. Rao, E. Richter, M. Menon, A. Rinzler, R.E. Smally, and P.C Eklund, Phys. Rev. B. **59**, 10 928 (1999).
[28] J. Cambedouzou, J.-L. Sauvajol, A. Rahmani, E. Flahaut, A. Peigney, and C.Laurent Phys. Rev. B 69, 235422 (2004):
[29] A. Rahmani, J.-L. Sauvajol, J. Cambedouzou, and C. Benoit Phys. Rev. B **71**, 125402 (2005)
[30] H. Chadli, A. Rahmani, K.Sbai, P. Hermet, S. Rols and J. -L. Sauvajol, Phys. Rev. B **74**, 205412 (2006)